THERMOFLUID OPTIMIZATION OF A HEATED HELICOPTER ENGINE COOLING BAY SURFACE

D. Wang [1], G. F. Naterer [2], G. Wang [3]
Department of Mechanical and Industrial Engineering
University of Manitoba, 15 Gillson Street
Winnipeg, Manitoba, Canada, R3T 2N2

ABSTRACT

In this paper, a global optimization technique based on the Adaptive Response Surface Method (ARSM) is integrated with a Control Volume Finite Element Method (CVFEM) for thermofluid optimization. The objective of the optimization is to improve the thermal effectiveness of an aircraft de-icing strategy by re-designing the cooling bay surface shape. The design optimization combines the modeling of heat conduction and potential fluid flow to investigate the complex thermofluid phenomena at the engine cooling bay. Based on the comparison between the ARSM predicted results and the plotted objective function, it is observed that the integrated technique provides an effective method for thermofluid optimization. The current method of integrating heat conduction, fluid flow, and optimization techniques shows a promising potential for subsequent extensions to more complex Multidisciplinary Design Optimization (MDO) problems. In addition, a novel pre-optimization technique is developed, and optimization results are presented and validated for the helicopter engine cooling bay problem.

[1] Ph. D. Student. Department of Mechanical and Industrial Engineering, University of Manitoba, Canada.
[2] Associate Professor. Department of Mechanical and Industrial Engineering, University of Manitoba, Canada.
[3] Assistant Professor. Department of Mechanical and Industrial Engineering, University of Manitoba, Canada.

Nomenclature

AR	aspect ratio
c_p	specific heat
h	convection coefficient
k	thermal conductivity
N	interpolation (shape) function
r	fraction of uniced surface area
s, t	local coordinates within element
T	temperature
u, v	velocity components
V	velocity
x, y	Cartesian coordinates
SCV	sub-control volume
SS	sub-surface
ip	integration point

Greek

b	regression coefficient
q	temperature difference
r	density
ϕ	velocity potential

Subscripts

a	air
f	fluid
g	gas
i	node number
w	wall

I. INTRODUCTION

Due to increased industrial competition for more efficient processes, a growing emphasis is placed on design optimization. In the design of external aircraft surfaces, shape is an important factor, but various trade-offs involving other factors must be considered. For example, the engine intake scoop of a helicopter cooling bay can be ice prone under certain atmospheric conditions. Its effective shape design involves a complicated trade-off between aerodynamic drag, ice protection and other factors (i.e. cost, manufacturing, and efficiency). In particular, shape optimization could be applied in a way to reduce droplet capturing and ice buildup on an aircraft surface. For example, various modifications of the surface profile could be used for passive shedding of runback water before it refreezes near the engine intake. In this way, an optimized geometrical configuration can lead to improvements in engine efficiency and aircraft controllability. Better ice-protected designs would improve the commercial viability, safety and endurance of flight in winter weather conditions. Although these wide-ranging objectives are beyond the scope of this paper, an optimization technique will be developed and applied to a specific sub-component of the overall problem described herein.

Search methods, based on the selection of a best design from several alternatives, are widely used for the optimization of thermal and fluid engineering systems (Jaluria [1]). Also, geometric shape optimization arises in many practical problems, such as aircraft wing profile design. Genetic algorithms (Sharatchandra et al. [2]) and NURBS (non-uniform rational B-splines) have been applied successfully to optimize geometric designs in aerospace applications [3]. Optimization methods based on multi-variable calculus and Lagrange multipliers [1] are generally limited to analytical functions, whereas many practical problems require a discrete approximation of the surface and governing equations. Recent developments have indicated that an optimization based on the method of 'design of experiments' (DOE) (Haftka et al. [4]) can offer substantial advantages over conventional methods. It is anticipated that this approach could offer new insight into designing more effective aircraft de-icing systems. In this type of search method, an objective function is optimized based on its evaluation at carefully selected experimental points.

Despite recent advances in this approach, certain limitations are still encountered. For example, a rapid rise of computational time is anticipated when the number of adjustable design parameters, n, is increased. However, in view of its promising potential in other regards such as MDO, the numerical optimization technique based on DOE will be considered in this article. In this approach, several simulations involving finite element analyses with different geometric configurations and other parameters are performed. A global optimization method developed for computationally intensive design problems, namely the ARSM, is applied for the design optimization [5, 6].

The Adaptive Response Surface Method (ARSM) fits a quadratic approximation model (called a response surface or surrogate) to the design objective function with a group of real experimental design points by calling a finite element solver. The design space and surrogate are then gradually refined until the optimum point converges within a desired small design space. The final optimal value of the objective function is calculated based on the design variables corresponding to the optimum point of the surrogate by calling the finite element solver again. The ARSM can significantly reduce

the total computational cost in finding the global or close-to-global optimum. In this work, numerical formulations of heat conduction and potential flow [9, 10] are integrated with the ARSM. The formulations are successfully applied to an application involving heat input and external flow past an iced aircraft surface.

II. NUMERICAL FORMULAION

Both heat conduction and potential flow problems can be described by Laplace's equation, which is shown as follows [9],

$$\frac{\partial \varphi^2}{\partial x^2} + \frac{\partial \varphi^2}{\partial y^2} = 0 \qquad (1)$$

In Eq. (1), φ represents temperature, T, for two-dimensional steady heat conduction, without internal heat sources, or velocity potential, ϕ, for external potential flow. In particular, the governing equation for two-dimensional heat conduction is given by

$$k\left(\frac{\partial^2 T}{\partial x^2} + \frac{\partial^2 T}{\partial y^2}\right) = 0 \qquad (1a)$$

and the governing equation for two-dimensional potential flow is given by

$$\frac{\partial \phi^2}{\partial x^2} + \frac{\partial \phi^2}{\partial y^2} = 0 \qquad (1b)$$

where $\phi = \phi(x, y)$, $u = \frac{\partial \phi}{\partial x}$ and $v = \frac{\partial \phi}{\partial y}$.

Although detailed flow predictions often require the full Navier-Stokes equations (i.e. Naterer [25]), rather than the simplified potential flow equations, a main purpose of this article is establishing a new framework for combined thermal / fluid optimization. Once established and validated, suitable extensions to viscous, turbulent flows can be developed. Also, analytical solutions of Eq. (1) are only

available for limited geometries. As a result, numerical solutions are often required, particularly for problems involving complex geometries. In the present work, a numerical solution of Eq. (1) is obtained by a CVFEM (Control-Volume-Based Finite Element Method), based on Refs. [9, 10].

In the CVFEM, the two-dimensional solution domain is subdivided into an assembly of linear, quadrilateral, isoparametric finite elements and control volumes (see Fig. 1). A control volume consists of four SCVs (sub-control volumes) from elements surrounding a particular global node that uniquely identifies the control volume. Since Eq. (1) is discretized within each element, the discrete equations are formed locally and independently of the overall mesh configuration. Assembly rules are carried out by conventional finite element procedures [11].

The transformation between local and global variables, as well as interpolation of scalar values within an element, are performed through bilinear shape functions. These shape functions are denoted by $N_i(s, t)$, where the subscript i refers to local node, and s and t refer to local coordinates (see Fig. 1). The value of φ and global coordinates corresponding to a local coordinate, (s, t), can then be approximated by

$$\varphi(s,t)=\sum_{i=1}^{4}N_i(s,t)\varphi_i \tag{2a}$$

$$x(s,t)=\sum_{i=1}^{4}N_i(s,t)x_i \tag{2b}$$

$$y(s,t)=\sum_{i=1}^{4}N_i(s,t)y_i \tag{2c}$$

where

$$N_1(s,t)=\frac{1}{4}(1+s)(1+t) \tag{3}$$

$$N_2(s,t)=\frac{1}{4}(1-s)(1+t) \tag{4}$$

$$N_3(s,t)=\frac{1}{4}(1-s)(1-t) \tag{5}$$

$$N_4(s,t)=\frac{1}{4}(1+s)(1-t) \tag{6}$$

The subscripts are i = 1, 2, 3 and 4 for the four local nodes within a linear, quadrilateral element.

Based on these definitions, the numerical solution can be obtained by spatial integration of Eq. (1) over a control volume, *cv*, yielding

$$\sum_{e,j} Q_{e,j} = 0 \qquad (7)$$

where the summation refers to the elements surrounding the global node (i.e., e = 1, 2, 3, 4 for internal nodes). Also, summation over j denotes the two surfaces of the sub-control volume within an element (note: not common edges of the sub-volumes within a control volume. See Fig. 1). The heat flow (or flow rate for a potential flow problem) across a surface is represented by

$$Q = \int_S \vec{q} \cdot \overrightarrow{dn} \qquad (8)$$

where $\overrightarrow{dn}$ is the surface normal and the heat flux vector (or flow rate per unit area), $\vec{q}$, is given by

$$\vec{q} = -k \frac{\partial \varphi}{\partial x} \vec{i} - k \frac{\partial \varphi}{\partial y} \vec{j} \qquad (9)$$

where k represents thermal conductivity for heat conduction, or air density for potential flow. Boundary conditions are applied along the external boundaries of the problem domain. In particular, for the heat conduction problem, convective boundary conditions are applied as follows,

$$q_w = -k \left. \frac{\partial T}{\partial n} \right|_w = h(T_f - T_w) \qquad (10)$$

where the subscripts w and f refer to wall and freestream fluid, respectively. Each boundary element contains 2 global nodes along the external boundary, except corners with 3 global nodes on the boundary. Heat flows are supplied at the boundary surfaces to complete the heat balances in the boundary control volumes. For example, the convective heat flow supplied at the boundary, based on Eq. (10), is given by

$$Q = \int_S h(T_f - T_w) \sqrt{\Delta x^2 + \Delta y^2} \qquad (11)$$

where the latter term (within the square root) represents the surface length of the boundary surface in that element. The values of Δx and Δy are determined from the shape functions, Eqs. (2) – (6), and the

local coordinates at each boundary node. The boundary heat flows from Eq. (11) are added to Eq. (7). In this way, the T_w portion becomes an active term on the left side of the global system of equations, whereas the T_f component is moved to the right side of the global system (i.e., constant; not multiplying any active temperature variables). In the following section, the implementation of an optimization method (ASRM) with the finite element solver will be described.

III. OPTIMIZATION PROCEDURE

The Adaptive Response Surface Method (ARSM) is a global optimization technique. The procedure of the ARSM consists of the following three main parts: (i) experimental design and modeling, (ii) design space reduction, and (iii) global optimization.

(i) Experimental Design; Latin Hypercube Designs

The first part of the ARSM is the experimental design. In this step, the data points of the independent variables are prepared in the design space, called experimental designs. This step is carried out through a formal planning strategy, called Latin Hypercube Designs (LHD) [12 - 16]. The objective function's value at the points is evaluated through the computationally intensive analysis and simulation process. In our case, this analysis refers to the CVFEM described in the previous section. Then, the objective function values are fitted by using the least squares method to build a regression model, called the response surface, or surrogate.

In the LHD approach, the range of each variable is evenly divided into n intervals, which usually depends on the model fitting method. For the least squares method, the value of n should be greater or equal to $(n_{var}+1)(n_{var}+2)/2$, where n_{var} is the number of independent variables of the objective function, to fit a complete quadratic model. Then, one observation is made in each input variable interval using random sampling within each interval. Thus, there are n observations for each input variable. Finally, each observation of one variable is combined with the other variables' observations only once and

used to calculate the objective function value by calling the finite element solver. When the variables' spans are reduced, only those observations that fall into the new variables' bounds would be re-used to generate the new surrogate [5].

(ii) Identification of the Reduced Design Space

In this paper, the objective function will involve a temperature difference (between engine burning gas and component), ΔT, in view of optimizing the thermal effectiveness of an aircraft de-icing configuration. This application will be described in greater detail in section IV. In this section, the objective function is modified (denoted by an over-tilde notation) while carrying out the mathematical optimization. In particular, the ARSM uses a second-order polynomial function as the response surface model, i.e.,

$$\tilde{\Delta T} = \beta_0 + \sum_{i=1}^{n} \beta_i x_i + \sum_{i=1}^{n} \beta_{ii} x_i^{\,2} + \sum_{i<j} \sum_{j=1}^{n} \beta_{ij} x_i x_j \qquad (12)$$

where β_i, β_{ii} and β_{ij} are regression coefficients. Also, x_i (i=1,2, … n) are design variables, including wall heat flux, q_w, and geometric parameters defining the shape of the cooling bay, while the objective function is $\tilde{\Delta T}$. The procedure of reducing the design space involves individually evaluating the maximum and minimum of each independent variable, while the other variables vary in their respective bounds.

Rearranging Eq. (12) gives the following quadratic function in x_k, with respect to other design variables,

$$\beta_{kk} x_k^{\,2} + (\beta_k + \sum_{i=1,<k}^{n} \beta_{ik} x_i + \sum_{i>k}^{n} \beta_{ki}\, x_i)\, x_k + [\sum_{i=1,\neq k}^{n} (\beta_{ii} x_i^{\,2} + \beta_i x_i) + \sum_{i<j,\neq k}^{n} \sum_{j=1,\neq k}^{n} \beta_{ij} x_i x_j + \beta_0 - \Delta \tilde{T}\,] = 0 \qquad (13)$$

This equation can be re-written as

$$ax_k^2 + bx_k + c = 0 \tag{14}$$

where

$$a = \beta_{kk}$$

$$b = \beta_k + \sum_{i=1,<k}^{n} \beta_{ik} x_i + \sum_{i>k}^{n} \beta_{ki} x_i \tag{15}$$

$$c = \sum_{i=1,\neq k}^{n} (\beta_{ii} x_i^{\,2} + \beta_i x_i) + \sum_{i<j,\neq k}^{n} \sum_{j=1,\neq k}^{n} \beta_{ij} x_i x_j + \beta_0 - \tilde{\Delta T}_0$$

The two solutions of x_k are given by

$$\left.\begin{matrix} x_{k,1} \\ x_{k,2} \end{matrix}\right\} = \frac{-b \pm \sqrt{b^2 - 4ac}}{2a}, \qquad (a \neq 0) \tag{16}$$

The reduced range of x_k is identified by the maximum and minimum of x_k with respect to the other design variables. Two subsidiary optimization problems are formulated as follows.

(1) For the lower limit of x_k ,

Minimize $\min\{x_{k,1}, x_{k,2}\}$

Subject to $x_{l,i} \le x_i \le x_{u,i} \quad (i = 1, \cdots, k-1, k+1, \cdots, n)$ (17)

where $x_{l,i}$ and $x_{u,i}$ are the lower and upper limits of x_i, respectively, from the previous model.

(2) For the upper limit of x_k ,

Minimize $-\max\{x_{k,1}, x_{k,2}\}$

subject to $x_{l,i} \le x_i \le x_{u,i} \quad (i = 1, \cdots, k-1, k+1, \cdots, n)$ (18)

When the response surface is reduced, the value of the threshold is essential because excessive reduction may remove the optimum. Usually, the second largest value is chosen within the span of design points. If the first cutting does not reduce the design space, we choose the next closest value,

which is less than the previous threshold, as the new threshold, until the ratio of the difference between the old and new design space is about five percent.

(iii) Global Optimization

The ARSM employs two existing global optimization algorithms to search for the minimum of the surrogate and the reduced space. The two algorithms are the 'Simulated Annealing' (SA) and the Boender-Timmer-Rinnoy-Kan (BTRK) clustering algorithm by Tibor Csendes [21, 22]. These two methods only need the objective function in the optimization; no gradient information of the objective function is required. The SA process is a stochastic optimization method analogous to the physical annealing of a solid. The BTRK clustering method was tested against other stochastic optimization algorithms including the SA, and the BTRK method was the winner for 45 standard testing problems of dimensions 2 - 30 [23]. In this work, the optimization problem was solved by the ARSM incorporating the BTRK.

Once the optimum of the surrogate was obtained, the real objective function value at the optimum is determined through an evaluation of the computationally intensive objective function. If the optimum is within the new design space, the point is added to the set of experimental designs for the following iteration. For each surrogate, a threshold, or cutting value, is used to reduce the design space. The design area is reduced in the direction of each variable. The next iteration starts with a new surrogate and repeats the above process until the span of all variables is sufficiently small. The global optimum value is the minimizer of the problem. The detailed framework of the ARSM is shown in Fig. 2.

In the next section, the previously described ARSM, as well as the finite element solver (CVFEM), will be applied to the thermal analysis of an engine cooling bay.

APPLICATION PROBLEM

This section consists of the following five main parts: (i) problem description, (ii) objective function, (iii) geometry generation, (iv) physical analyses and boundary conditions for heat transfer and potential flow and (v) mesh generation.

(i) Problem Description

In a helicopter, outside air is forced into the engine cooling bay through a separate intake (see Fig. 3 – (b)). Under certain atmospheric conditions, the intake scoop is often ice prone, and so it can be heated to reduce or prevent ice buildup on the intake scoop. As the air flows into the intake and over the various engine components, it experiences considerable drag forces (often up to 25 – 30 % of the total drag) due to pressure, frictional and ice blockage effects. Also the intake scoop should allow enough airflow to satisfy the engine performance requirements. As a result, it is desirable to obtain an optimized shape design of the air intake scoop to reduce the drag and increase the engine efficiency, while preventing ice buildup through surface heating.

In this paper, the combined problem of icing and engine efficiency is considered. Since many complex parameters describe how engine systems actually operate, the intention here is to formulate the overall problem with simple model coefficients that identify certain overall trends. A closed form expression for the objective function is given and the ARSM can be tested in this regard. The coefficients in this objective function are not intended to represent a particular aircraft or engine, but rather, they are selected to yield certain expected physical trends. In this way, the suitability of the newly combined CVFEM-ARSM can be assessed.

In practical terms, ice on the helicopter intake scoop surface can be melted in two main ways. One way is to use bleed-air from a compressor to heat the scoop, while the other way uses electrical resistance heating. Generally, based on the material's thermal limit, the efficiency of the engine

depends on the temperature difference between engine burning gas and component ($\Delta T = T_g - T_w$), where a higher ΔT is considered to yield a better efficiency. This means that the temperature difference, ΔT, should be maximized. From the point of view of thermodynamics, reducing the amount of compressed air to heat the air intake scoop sufficiently is a way to improve the performance of the engine. Similarly, reducing the heat input of electrical resistance heating also can improve efficiency since the power required in such heating must be generated locally. On the other hand, less heating may cause more ice buildup on the intake scoop surface, which may break off (damaging downstream hardware), reduce the air inflow, and / or increase friction drag. Thus, these processes involve certain trade-offs in the aircraft design, thereby requiring an effective optimization.

(ii) Objective Function

The objective function of this problem, subject to the spans of design variables (see Fig. 3 – (a)), is

$$\Delta T = 1.59\left[T_{ad}(1-r^m)e^{-AR/n} - T_a\right]\left(\frac{\dot{m}_{in}}{\dot{m}_0}\right)^{0.34} \qquad (20)$$

This general functional form was motivated based on a curve-fitted cooling efficiency, as described by Hewitt et al. (1996). The curve fitted coefficients were derived for a convectively cooled surface representing an internal helicopter component. Other coefficients may be approximated to represent the physical trends and dependencies on the aspect ratio, *AR*, and uniced ratio, *r*. Such values could include other factors, such as incoming turbulence level, or pressure gradient. However, as discussed earlier, the coefficients were selected to represent certain expected trends, rather than the actual and detailed processes of the internal engine dynamics.

In Eq. (20), $\dot{m}_{in}$ ($\dot{m}_{in} = r\dot{m}$), AR and *r* are derived variables, where $\dot{m}_{in}$ is the air mass flow rate through the cooling bay intake, AR (aspect ratio of intake scoop) refers to the scoop height divided by the width, and *r* is the fraction of the un-iced area (above 273 *K*) to the total area of the intake scoop

exposed to air. In particular, AR=($y1$+$y2$)/0.1 (note: 0.1 is the width of the intake scoop at the bottom). The spans of design variables are specified as follows,

$$5500\ W/m^2 < q_w < 7500\ W/m^2$$

$$0.012\ m < x1 < 0.029\ m$$

$$0.017\ m < y1 < 0.039\ m$$

$$0.007\ m < x2 < 0.024\ m$$

$$0.007\ m < y2 < 0.029\ m \qquad (21)$$

In these inequalities, q_w is the heat flux across the bottom of the intake scoop (see Fig. 4 - (b)), and $x1$, $y1$, $x2$ and $y2$ are the coordinate values of control point 1 (CP1) and control point 2 (CP2), respectively, as shown in Fig. 3 – (a).

(iii) Geometry Generation

The geometry of the intake scoop was generated by Pro/Engineer 2000i [24]. A B-spline curve (see Fig. 3 – (a)) was used to plot the top surface of the intake scoop, since it has local properties. The whole B-spline curve is plotted based on seven control points (CP1, CP2, …., CP7), in which only two points (CP1 and CP2) were chosen as design variables for the optimization process. The geometric dimensions of CP1 and CP2 are set as relative coordinates. This simplifies the geometric constraints for the optimization process (see Fig. 3 – (a)). The reason to choose CP1 and CP2 as design points is that both of them can change the height and width of the scoop. The left segment of the scoop surface is more influential than other sections of the scoop surface on the incoming air through the intake port. Also, two explicit relationships are defined by

$$y3 = y4 = 1.1(y1 + y2);$$

$$y5 = 0.65(y1 + y2) \qquad (22)$$

where $y3$, $y4$ and $y5$ are respective dimensions of CP3, CP4 and CP5 along the y coordinate direction. This relationship can keep the shape of the scoop consistent with different combinations of $x1$, $y1$, $x2$ and $y2$.

(iv) Physical Analyses and Boundary Conditions for Heat Transfer and Potential Flow

The air mass flow rate, $\dot{m}$, depends significantly on the width of the intake port and the height of the intake scoop. A bigger width and larger height will allow greater air mass inflow. The fraction of the un-iced scoop area to the total area, *r*, is determined by both geometry of the scoop and the heat flux value, q_w. A smaller size of scoop needs less heat to deliver the same value of *r*. Several trends indicate that an optimum exists. For example, if $y1$, $y2$ become large and $x1$, $x2$ remain constant, then $\dot{m}$ increases, and so ΔT increases. On the other hand, the system will use more air (more heat) to melt the ice on the scoop surface. This is not desirable since excessive energy is extracted from the system for de- icing and ΔT likely decreases (per *kg* of fuel burned). A similar situation occurs with different $x1$ and $x2$. By running a pre-optimization process mathematically, it can be shown that the objective function is biggest when $r = 0.51$. This occurs with the same combination between AR and $\dot{m}$, regardless of AR and $\dot{m}$. More details about this pre-optimization will be discussed in section V.

In order to find *r* and $\dot{m}$, a heat transfer and potential flow simulation are respectively defined as shown in Figs. 3 – (b) and 3 – (a). For the heat transfer problem, the value of q_w is given as the uniform surface heat flux applied at the base of the intake scoop. The finite element solution of heat conduction with the CVFEM in the intake scoop will evaluate the temperature distribution therein. Convective boundary conditions are applied along all surfaces except the base of the intake scoop. The convection coefficient and other problem parameters are listed in the appendix. In this analysis, it is assumed that ice can accumulate on the intake surface when the surface temperature falls below zero degrees Celsius in the presence of incoming supercooled droplets.

The potential flow solution with the CVFEM gives the velocity field around the intake scoop. The velocity of upstream incoming (freestream) air, V_∞, which is parallel to the *x* direction, is specified at the left inlet. It is known that $\varphi = \varphi(x, y)$. At the right outlet, *x* is constant along the outlet boundaries. Thus, φ is only functionally dependent on *y* there. Also, the cross-stream velocity

component, *v*, is assumed to be zero at the right outlet, which means that φ is constant at that location. Also, the velocity potential is a relative value in the potential flow field. Thus, φ is arbitrarily set as 100 at the right outlet. Consider the same value of φ at the bottom outlet, as the potential flow simulation only focuses on how the geometry of the intake scoop influences the air mass inflow rate. In other words, the influences from other factors, such as boundary conditions, should be eliminated. This hypothesis was tested by running the same geometry of the scoop with different values of φ and different simulations (but same φ values at both outlets for each case), and then obtaining the same air mass flow results.

The boundary condition at the top of the domain is specified as

$$\frac{\partial \phi}{\partial x} = u = V_{\infty}$$

or

$$\frac{\partial \phi}{\partial y} = v = 0$$

It means that no air flow is perpendicular to the top boundary, provided that the height of the computational domain is sufficiently large. In this paper, this boundary condition, $\frac{\partial \phi}{\partial x} = u = V_{\infty}$, is called the Free Boundary Condition and the other one, $\frac{\partial \phi}{\partial y} = v = 0$, is called the Zero Gradient Boundary Condition. Zero flux conditions are specified at the other boundaries, i.e. $\frac{\partial \phi}{\partial n} = 0$.

Actual aircraft icing processes involve viscous effects, phase change heat transfer, impinging droplets and other complex thermofluid processes [25, 26]. However, the main purpose of this article is to determine whether an ARSM optimization can be effectively combined with a coupled heat transfer / fluid flow solver. Despite the limitations of a potential flow solution, it is expected to provide

reasonable trends for a main parameter of interest, namely, the intake flow rate. Also, very few (or no) previous studies have attempted to combine the three parts (heat transfer, fluid flow, optimization) simultaneously, in such ways. Once validated, the combined algorithm will serve as a solid foundation, from which future extensions involving droplet dynamics, etc., can be incorporated.

(v) Mesh Generation

All meshes for the CVFEM simulation were created by ANSYS 6.0 [27] after importing a geometry file from Pro/Engineer with IGES format to ANSYS, as shown in Figs. 8 – (a) and 8 – (b). Regarding the numerical calculations, convergence is always a prerequisite condition of any final result. The resolution of the mesh (element edge length), instead of the number of mesh elements, is chosen here as a convergence criterion since the resolution of the mesh is independent of the size of the domain. The computational results should be independent of the grid, as the results should be the same regardless of the grid selected for a particular case. The potential flow is used in the convergence study. The height and length of the computational domain were set by 0.15m and 0.35m, respectively, for the convergence study. Results are shown in Fig. 5 – (a). A resolution of $0.013m$ (element edge length) is observed to be sufficient for all meshes of the external flow simulation. For heat transfer calculations, the resolution is $0.00325m$.

Under the case of a uniform ϕ at both outlets, the air mass flow rate becomes independent of the length of both outlets, L1 and L2, provided that both lengths can enclose the computational area. The lengths of L1 and L2 are respectively set as 0.4m and 0.14m, as shown in Fig.4 – (a).

For the potential flow, the streamlines are parallel to each other. Thus, the amount of air flowing through each outlet depends on where the stagnation point on the intake scoop is located. Furthermore, we can consider that the position of the stagnation point, which should be located at the leading edge of the intake scoop, will only depend on the geometry of the intake scoop, when the height of the computational domain exceeds a certain value with free top boundary conditions, because a small

height of the intake scoop will reduce the external flow portion. On the other hand, due to the specified boundary conditions of potential flow, we can interpret the external flow case as a duct or channel type flow. They (applied potential flow and duct flow) have an analogous type of boundary conditions, as the height of the computational domain is big enough, so that there is no air mass flux across the top boundary. The x component of air velocity is equal to the freestream air component at the top of the computational domain. So, the role of the intake scoop resembles a valve in pipe flow, as the computational domain resembles a tee junction with one inlet and two outlets. It means that some geometry of the scoop (according to a certain position of the valve) will generate a high flow rate, regardless of the height of the domain (according to the diameter of the pipe).

A useful purpose of the potential flow simulation is to find how the geometry of the scoop influences the air mass flow rates. The results of the studies appear to be acceptable if all external flow simulations maintain the same general trend. This trend shows the same sequence for different geometries of the intake scoop, from the biggest air mass flow rate to the smallest rate. The sequence should represent the actual order, regardless of whether the detailed airflow values are specifically correct.

Due to the above considerations, we can apply the Zero Gradient Boundary Condition, $\frac{\partial \phi}{\partial y} = v = 0$, at the top of the computational domain, reduce the height of the computational domain, H, and then decrease the number of elements, computational cost and time during the optimization process. Two schematics are shown in Fig. 5, and the value of $0.2m$ is set as the height of the computational domain during the optimization process (as shown in Fig. 4 – (a)). After finishing the optimization process, a big height of the computational domain ($0.5m$ high) is used to calculate $\dot{m}$ of the optimum case. This optimization strategy is summarized in Fig. 6.

Based on the optimization strategy of the ARSM, many intermediate experimental points are needed to fit the surrogate for cutting during the optimization process. Thus, the above simplification by using the low fidelity external flow modeling significantly reduces the total cost of the whole optimization. The total computational time of the external flow simulations with 0.5*m* height and free top boundary condition, $\frac{\partial \phi}{\partial x} = u = V_\infty$, is 9738*s*, while the reduced computational domain with 0.2m height and zero gradient top boundary condition, $\frac{\partial \phi}{\partial y} = v$ =0, requires 1628*s* (Pentium III 550 MHz, 256 MB memory).

IV. RESULTS AND DISCUSSION

The first example considers only heat transfer (without external flow simulations), together with approximated mass inflow modeling, and the ARSM for optimizing the helicopter engine cooling bay surface. The model uses the same objective function as Eq. (20), but only two design variables were considered, namely q_w and AR. The objective function is shown in Fig. 7 with respect to the two variables. By observing this result, it can be observed that the objective function is complex with many local optima.

Such complex functions present a great challenge to conventional local optimization techniques, such as gradient-based methods. Due to the required interactions with the computationally intensive FEA processes, stochastic global optimization methods, such as SA and GA, are not appropriate either. By applying the ARSM, the global optimum was obtained using only 45 function evaluations. The predicted optimum was validated through comparisons with the actual objective function plots. Additional details regarding such 2-variable studies are described in Ref. [20].

The next (second) test problem, represented by the same objective function, involves a coupled thermofluid problem with five design variables to be included. For this problem, the optimization procedure called the finite element solver 37 times during 4 iteration steps. One call includes the CVFEM heat transfer and potential flow simulations. Each iteration step corresponds to one response surface constructed by the ARSM. An example plot of the spatial temperature distribution (subject to different $x1$, $y1$, $x2$, $y2$ and q_w values) is shown in Fig. 8 – (c). An example of the external potential flow field (subject to different x1, y1, x2 and y2) is shown in Fig. 8 – (d). The heat transfer and flow simulation processes yield the values of r, AR and $\dot{m}$ in calculating the objective function value.

The results from each CVFEM simulation were passed to the ARSM modules to reduce the design space until a final optimal value was determined. The optimum value was obtained during the 22nd call to the CVFEM in the first iteration step of the whole optimization process, while retaining this same value in the rest of the iteration steps. The final optimum, ΔT, is 1899.37K, when $x1$=0.015m, $y1$=0.025m, $x2$=0.007m, $y2$=0.022m, q_w=5701W/m^2, AR=0.47, r=0.5002 and $\dot{m}$ =6.399kg/s, as shown in Fig. 9 – (c) with a view scale of 2.0. The smallest and the biggest intake scoops are also shown in Figs. 9 – (a) and 9 – (b) with the same view scale of 2.0. The $\dot{m}$ value for the optimum was calculated based on a domain height of 0.5m (free top boundary condition).

The optimization results are validated by a pre-optimization process. The pre-optimization used loops to run the objective function, Eq. (20), based only on the three derived variables, AR, r and $\dot{m}$. A reasonable span of these three variables is first given as follows:

$0 < r < 1$

5.0 kg/s < $\dot{m}$ < 5.5 kg/s (subject to the computational domain of 0.2m height)

0.24 < AR < 0.68 (subject to the spans of $y1$ and $y2$)

By plotting Eq. (20), it was found that the objective function reaches the biggest value when r is 0.51, for a given combination of AR and $\dot{m}$. On the other hand, it means that the optimum of the objective

function is located at $r = 0.51$. Also, the objective function, ΔT, is proportional to the air mass flow rate, $\dot{m}$, which suggests a relatively large size of the intake scoop, thereby causing extra aerodynamic friction and heating. Furthermore, as the value of *AR* increases, the objective function value decreases at the same $\dot{m}$, as shown in Fig. 10 – (a). Using $\Delta T = 1780K$ (chosen from several available experimental points) as a threshold with a given $r=0.51$, all solutions are depicted in Figs. 10 – (b), 10 – (c) and 10 – (d), based on all combinations of *AR* and $\dot{m}$. It appears that the objective function over *1780K* only exists in the span of *AR* from *0.2* to *0.54*. This pre-optimization process can significantly reduce the span of *AR* in a comparison with the original span of *AR* (0.24 – 0.68). Thus, it can reduce the computational cost of the ARSM because it is sensitive to the number and span of design variables. For more design variables with larger spans, more experimental points and computational time are needed by the ARSM.

Figures 10 – (b), (c) and (d) show the results as inclined planes. The largest objective function value arises at a low *AR* area with a high $\dot{m}$. However, as expected in the real situation, the higher intake scoop and wider intake port lead to a high air mass flow rate, $\dot{m}$. Thus, a low *AR* implies that both the size of the intake scoop and the air mass flow, $\dot{m}$, are small. In other words, it suggests that this value of the objective function would not likely arise in practice. From Figs. 10 – (b), (c) and (d), the predicted optimum with the ARSM is considered to be acceptable since the difference between the theoretical optimum of 1786K (subject to a small computational domain of 0.2m height) and the real optimum (about 1810K, subject to a small computational domain of 0.2m height, based on the possible combinations of AR and $\dot{m}$) is reasonably small.

Thus, based on results from a 2-variable case, as well as results for a more complex, coupled thermofluid problem involving 5 design variables, the ARSM appears to perform effectively and efficiently when combined with a CVFEM for multi-modal objective functions.

V. CONCLUSIONS

In this paper, a Control-Volume-Based Finite Element Method (CVFEM) and an optimization technique, called the Adaptive Response Surface Method (ARSM), were integrated to find the optimal design of a complex thermofluid problem. The application involves heating of an iced surface on a helicopter engine cooling bay intake. To the best knowledge of the authors, it is the first endeavor to combine such heat transfer, fluid flow and optimization models simultaneously in search of the most desired engineering solution. The study also demonstrates that the ARSM can effectively and efficiently solve computationally intensive optimization problems with multiple local optima. The ARSM, as one of the DOE-based optimization methods, can be computed in parallel with multiple physical processes, such as heat and fluid flow during aircraft icing, to further reduce the computational time. Also, in this article, a novel pre-optimization procedure has been developed to improve simulation efficiency, with a potential to be generalized for other types of problems. Numerical results have been presented for an optimized scoop geometry, together with its corresponding heating requirements and air mass inflow. Based on the current study, the optimization algorithm is viewed to have promising potential for extensions to other Multidisciplinary Design Optimization (MDO) problems.

ACKNOWLEDGEMENTS

Financial support of this research project from the Natural Sciences and Engineering Research Council of Canada is gratefully acknowledged.

REFERENCES

[1] Jaluria, Y., *Design and Optimization of Thermal Systems*, McGraw-Hill, New York, 1998.
[2] Sharachandra, M. C., Sen, M., Gad-el-Hak, M., "*New Approach to Constrained Shape Optimization Using Genetic Algorithms*," *AIAA Journal*, vol. 36, no. 1, pp. 51 – 61, 1998.
[3] Trepanier, J. Y., Lepine, J. L., Pepin, F., "*An Optimized Geometric Representation for Wing Profiles Using NURBS*," *Canadian Aeronautics and Space Journal*, vol. 46, no. 1, pp. 12 – 19, 2000.

[4] Hafka, R. T., Scott, E. P., Cruz, J. R., "*Optimization and Experiments: A Survey*," *Applied Mechanics Reviews*, vol. 51, no. 7, pp. 435 – 448, 1998.
[5] Wang, G., "*Adaptive Response Surface Method Using Inherited Latin Hypercube Design Points*," *Transactions of the ASME, Journal of Mechanical Design* (in print), 2002.
[6] Wang, G., Dong, Z., Aitchison, P., "*Adaptive Response Surface Method – A Global optimization Scheme for Approximation-based Design Problems*," *Journal of Engineering Optimization*, vol. 33, no. 6, pp. 707 – 734, 2001.
[7] Kirkpatrick, S., Gelatt, C. D., Vecchi, M. P., "*Optimization by Simulated Annealing*," *Science*, vol. 220, pp. 671 – 680, 1983.
[8] Shih, T. M., *Numerical Heat Transfer*, Hemisphere Publishing Corporation, New York, 1984.
[9] Naterer, G. F., *Heat Transfer in Single and Multi-Phase Systems*, CRC Press LLC, Boca Raton, FL, 2002.
[10] Schneider, G. E., Zedan, M., P., "*Control Volume Based Finite Element Formulation of the Heat Conduction Equation*," AIAA Paper 82-0909, *AIAA / ASME 3rd Joint Thermophysics, Fluids, Plasma and Heat Transfer Conference*, St. Louis, Missouri, June 7 – 11, 1982.
[11] Reddy, J. *Introduction to the Finite Element Method*, McGraw-Hill, Inc., New York, 1984.
[12] McKay, M. D., Bechman, R. J., Conover, W. J., "*A Comparison of Three Methods for Selecting Values of Input Variables in the Analysis of Output from a Computer Code*," *Technometrics*, vol. 21, no. 2, pp. 239 - 245, May, 1979.
[13] Iman, R. L., Conover, W. J., "*Small Sensitivity Analysis Techniques for Computer Models with an Application to Risk Assessment," Communication Statistics - Theory and Methods*, A9 (17), pp. 1749 - 1842, 1980.
[14] Tang, B., "*Orthogonal Array-based Latin Hypercubes*," *Journal of American Statistical Association*, vol. 88, no. 424, Theory and Methods, pp. 1392 - 1397, 1993.
[15] Park, J. S., "*Optimal Latin-hypercube Designs for Computer Experiments," Journal of Statistical Planning Inference*, vol. 39, pp. 95 - 111, 1994.
[16] Ye, K. Q., Li, William, Sudianto, A., "*Algorithmic Construction of Optimal Symmetric Latin Hypercube Designs*," *Journal of Statistical Planning and Inferences*, 2000.
[17] Cheney, W., Kincaid, D., *Numerical Mathematics and Computing,* Brooks / Cole Publishing Company, Second Edition, 1985.
[18] Dong, Z., Xue, D., *Excerpts from Notes on Optimization*, University of Victoria, Canada, 1996.
[19] Hewitt, G. F., Shires, G. L., Polezhaev, Y. V. (ed.), *International Encyclopedia of Heat and Mass Transfer*, CRC Press LLC, 1996.
[20] Wang, D., Naterer, G. F., Wang, G., "*Adaptive Response Surface Method for Thermal Optimization: Application to Aircraft Engine Cooling System*," AIAA Paper 2002-3000*, AIAA / ASME 8th Joint Thermophysics and Heat Transfer Conference*, St. Louis, MO, June 24 – 27, 2002.
[21] Boender, C. G. E., Rinnooy, A. H. G., Kan, L. S. and Timmer, G. T. (1982), "*A stochastic method for global optimization*," Math. Progr. Vol. 22, pp. 125-140.
[22] Csendes, T., "*Two non-derivative implementations of Beender et al's global optimization method: numerical performance*," Report 1985/2, Jo`zsef Attila University, Szeged, Hungary, 1985.
[23] Neumaier, A., http://www.mat.univie.ac.at/~neum/glopt.html. Computational Mathematics group, the University of Vienna, Austria, 2002.
[24] *Fundamentals of Pro/Engineer 2000i*, Parametric Technology Company, PTC Worldwide Headquarters, 140 Kendrick Street, Needham, MA 02494, 718.370.5000, 2000..
[25] Naterer, G. F., "*Multiphase Flow with Impinging Droplets and Airstream Interaction at a Moving Gas / Solid Interface*," *Int. J. of Multiphase Flow*, vol.28, no.5, pp.451-477, 2002.
[26] Naterer, G. F., "*Energy Balances at the Air / Liquid and Liquid / Solid Interfaces with Incoming Droplets at a Moving Ice Boundary*", *Int. Comm. Heat Mass Transfer*, vol.29, no.1, pp.57-66, 2002.
[27] *ANSYS 6.0 Online Help*, ANSYS Inc., Southpointe, 275 Technology Drive, Canonsburg, PA 15317.

APPENDIX

The following parameters were adopted in the example problem:

$\dot{m}_{in}$ = air mass flow rate through intake port ($\dot{m}_{in} = r\dot{m}$),

$\dot{m}_0$ = reference air mass flow rate, 5.6 *kg/s* ($\dot{m}_0 = V_\infty W_{in} \rho$, W_{in} indicates the width of the air intake port),

$\dot{m}$ = air mass flow rate through intake port (without considering ice prone on the intake surface) calculated by potential flow, with respect to different values of x1, x2, y1 and y2,

T_g = gas temperature past engine component,

T_a, T_∞ = freestream air temperature (253 *K*),

T_w = engine component temperature,

AR = aspect ratio (intake scoop height, H=*y*1+*y*2, divided by *W* = 0.1 *m*),

V_∞ = air velocity (40 *m/s*),

h = air convection coefficient (160 W/m^2K),

r = *r*(*x*1, *y*1, *x*2, *y*2, q_w) is the fraction of the un-iced area (above 273 *K*) to the total area of the intake scoop exposed to air (as determined from the CVFEM),

T_{ad} = 1,900 *K*,

ρ = air density (1.4 kg/m^3),

k = thermal conductivity (177 *W/mK*),

m = *4*, *n* = *10* (correlation coefficients of objective function),

W= width of intake scoop at the base (0.1*m*)

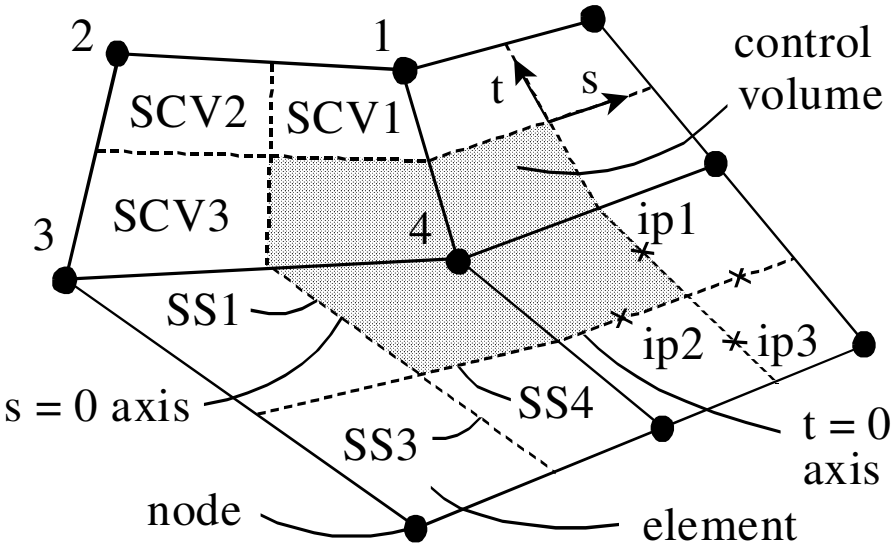

Figure 1 – Schematic of finite element and control volume in the CVFEM

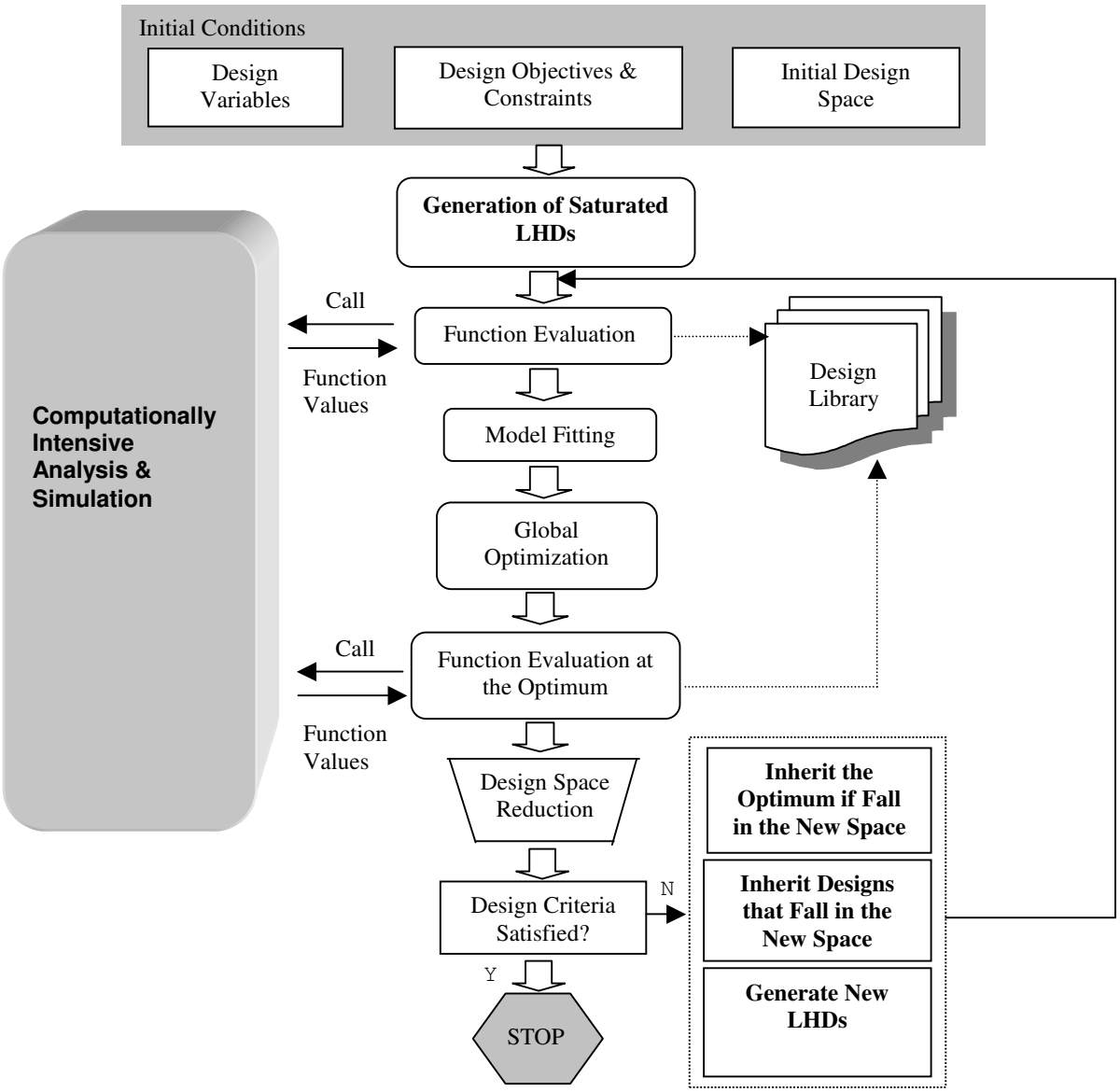

Figure 2 – Flowchart of the Adaptive Response Surface Method

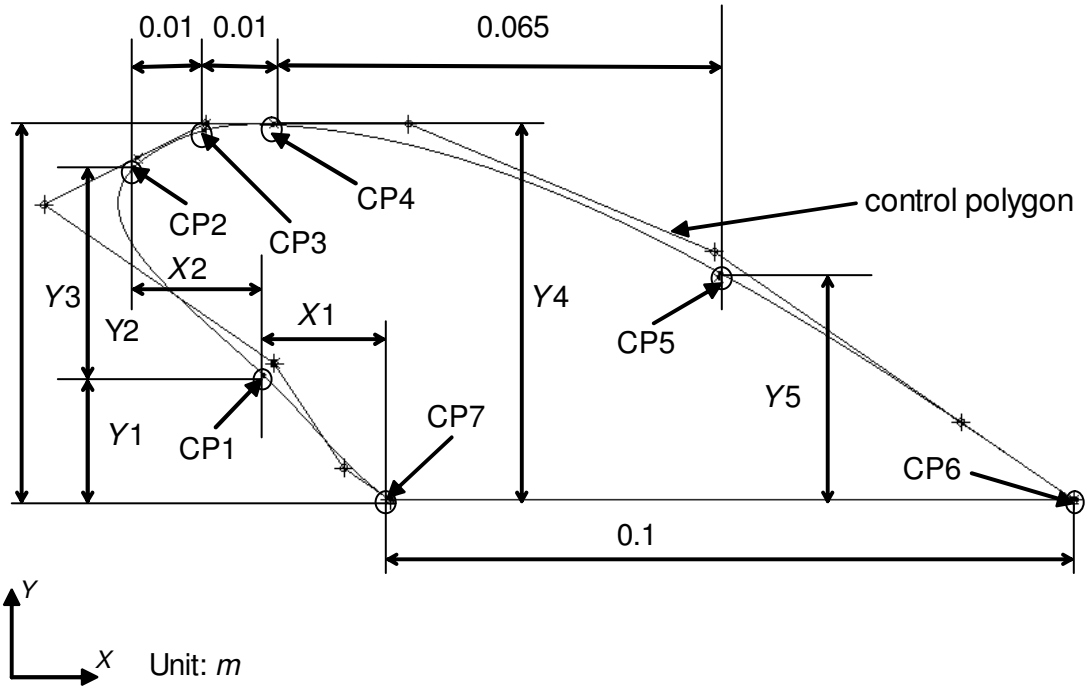

Figure 3 – (a) – Scoop shape created by B-spline curve

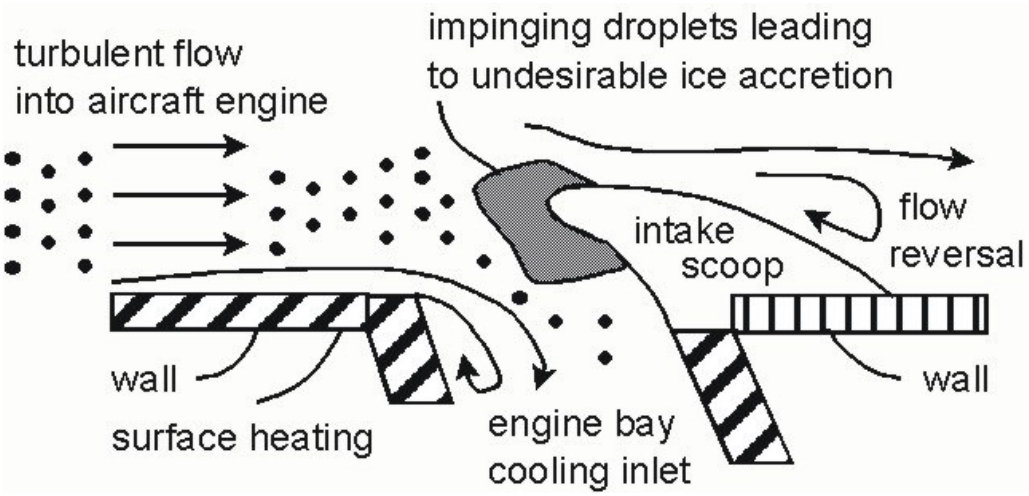

Figure 3 – (b) – Schematic of engine intake flow

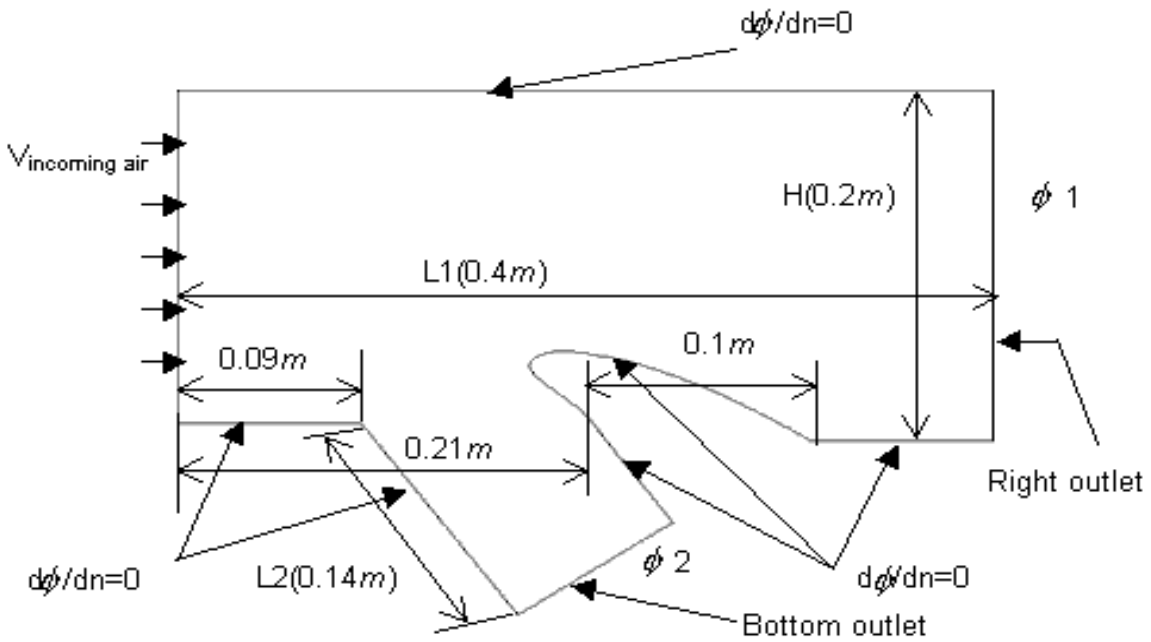

Figure 4 – (a) – Schematic of external flow problem

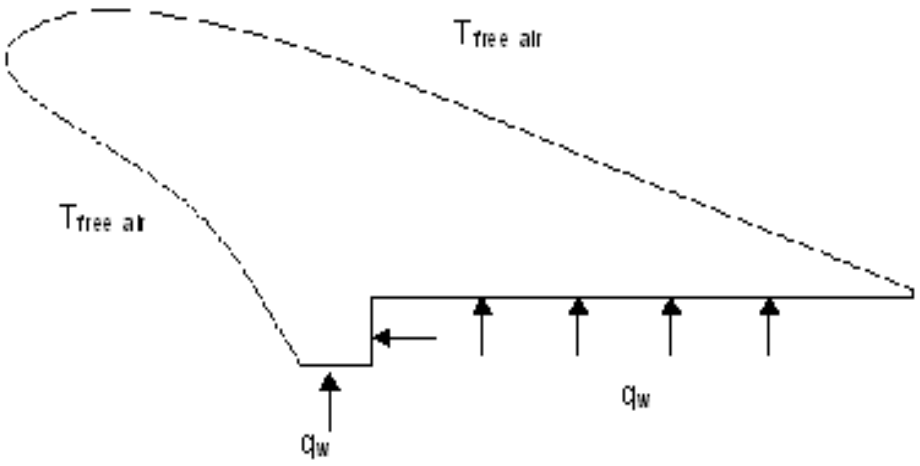

Figure 4 – (b) – Schematic of heat transfer problem

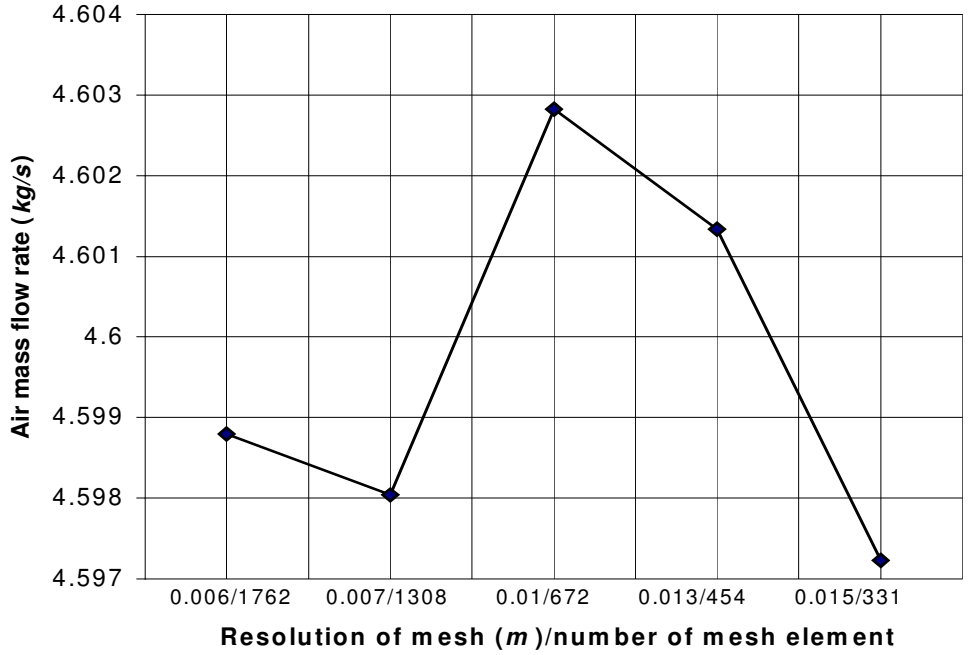

Figure 5 – (a) – Air mass flow rates at different mesh resolutions

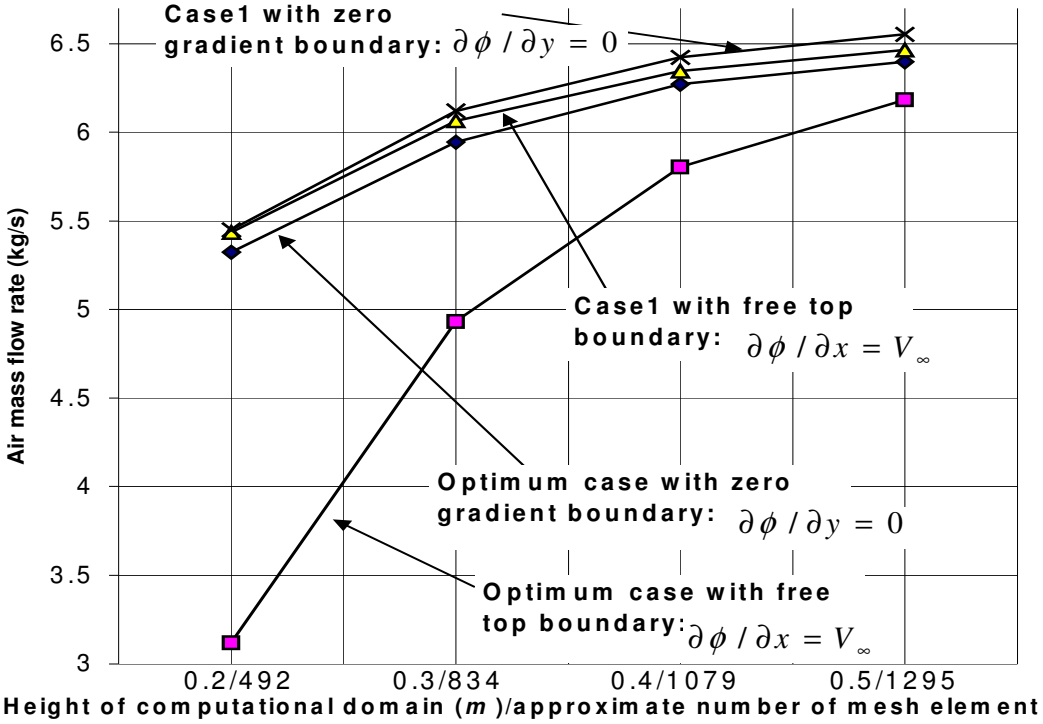

Figure 5 – (b) – Air mass flow rates with different domain heights and top boundary conditions

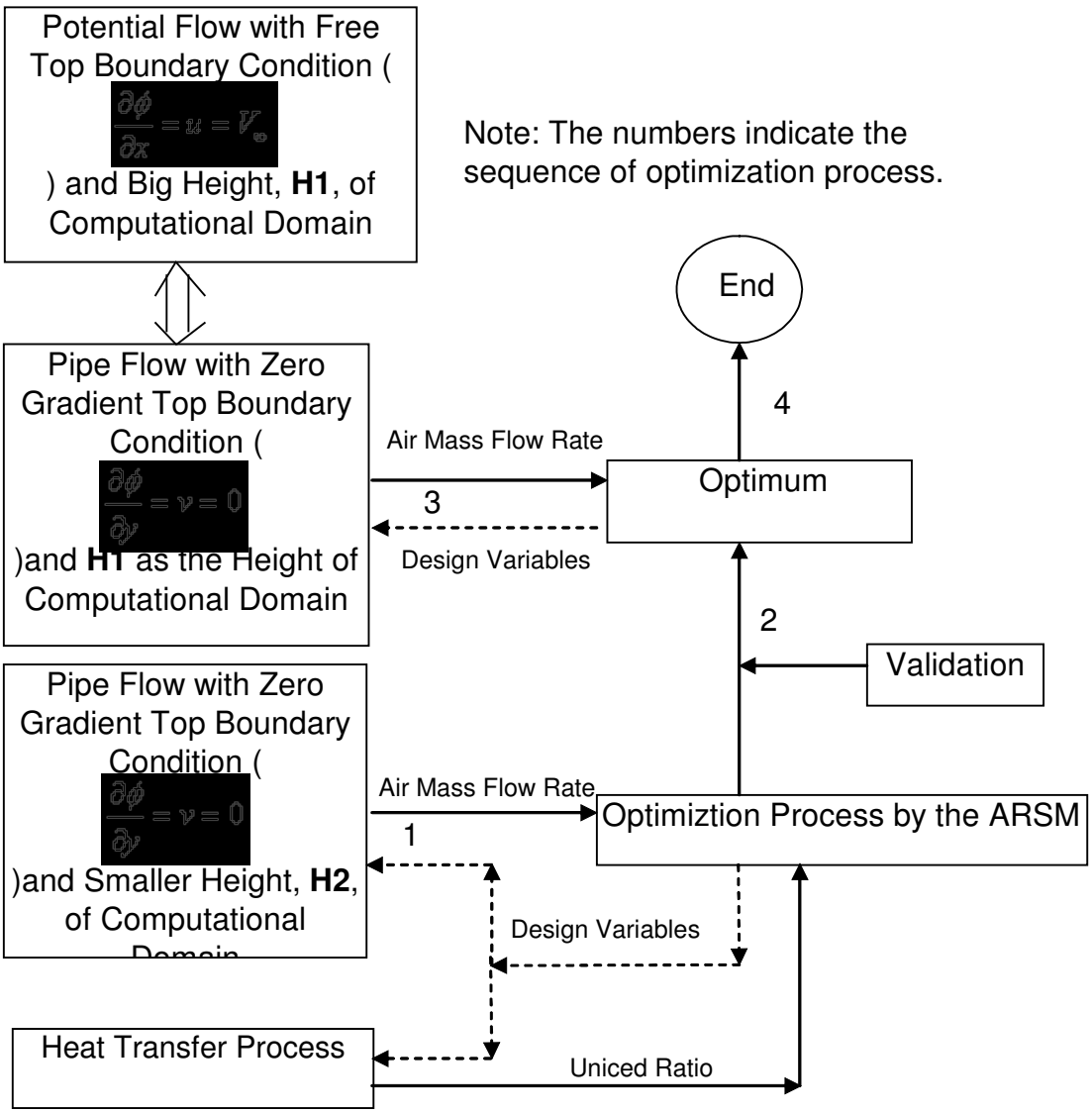

Figure 6 - Optimization strategy for fluid flow

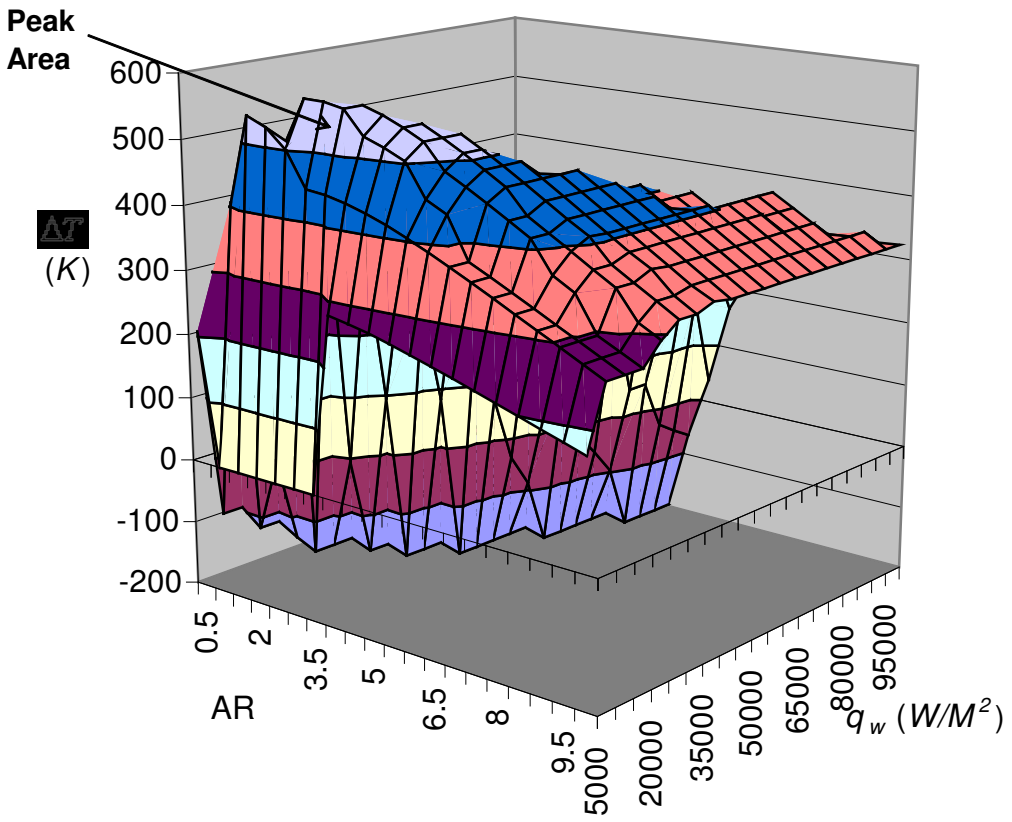

Figure 7. Objective function for 2-variable problem

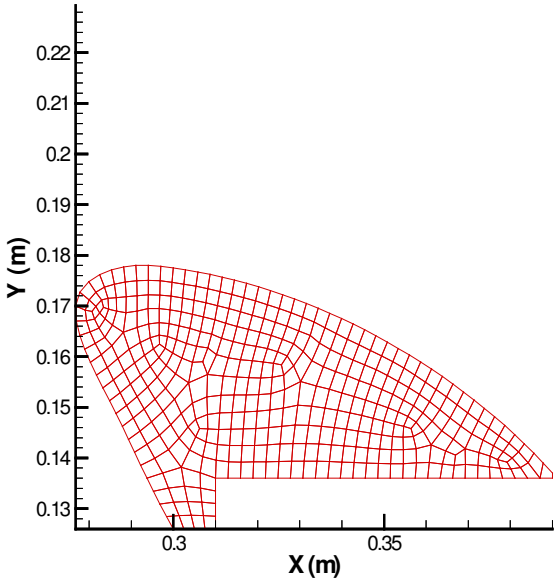

Figure 8 – (a) – Mesh for heat transfer problem with 0.00325 *m* resolution and 381 elements

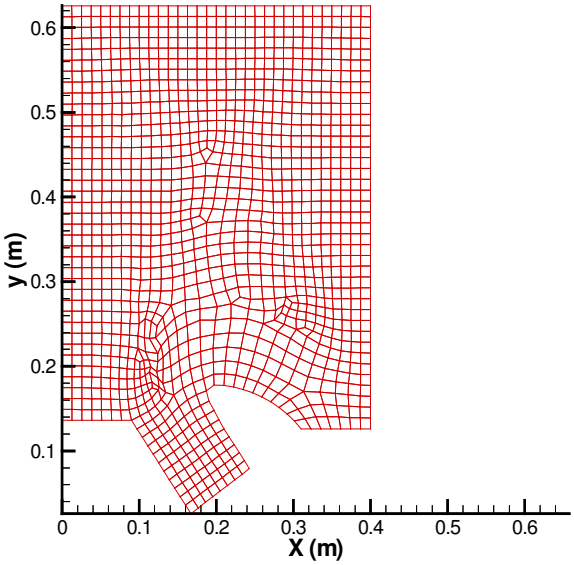

Figure 8 – (b) – Mesh for potential flow with 0.013 *m* resolution and 1213 elements

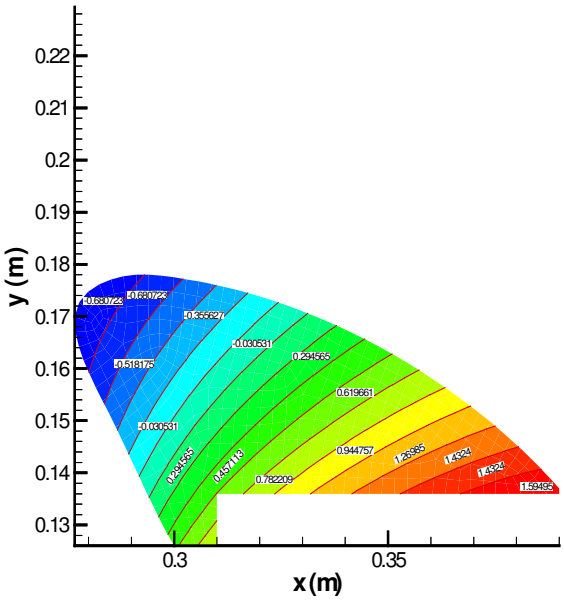

Figure 8 – (c) – Temperature distribution within the intake scoop

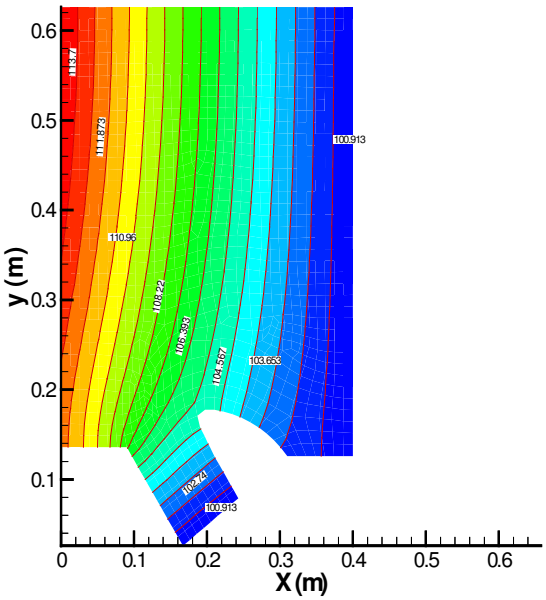

Figure 8 – (d) – Contours of velocity potential for the external flow field

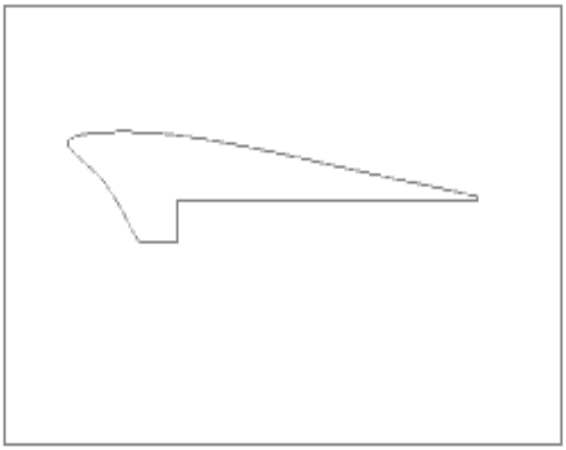

Figure 9 – (a) – Smallest intake scoop shape

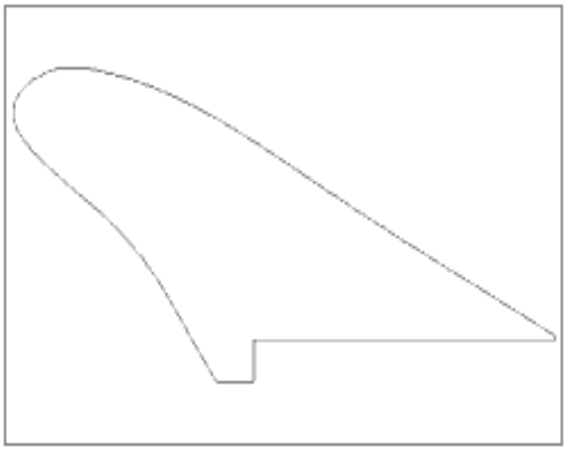

Figure 9 – (b) – Biggest intake scoop shape

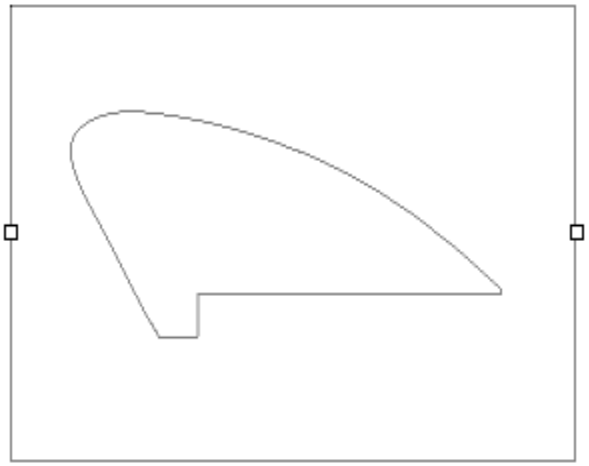

Figure 9 – (c) – Optimal intake scoop shape

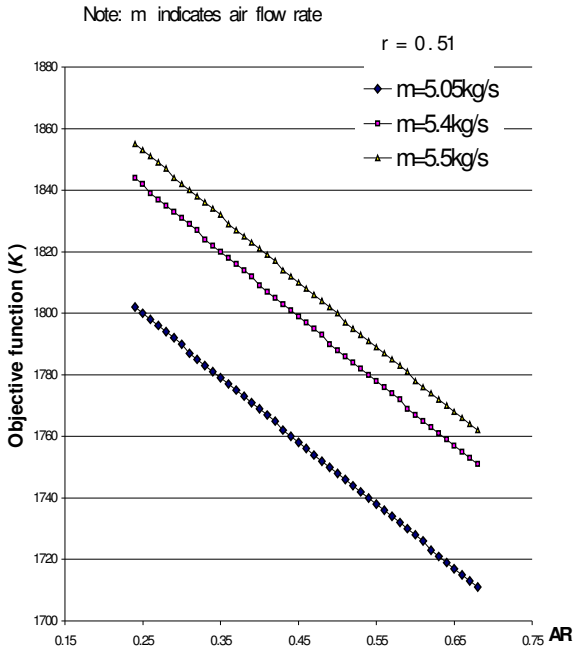

Figure 10 – (a) – Objective function versus AR and air mass flow rate, m

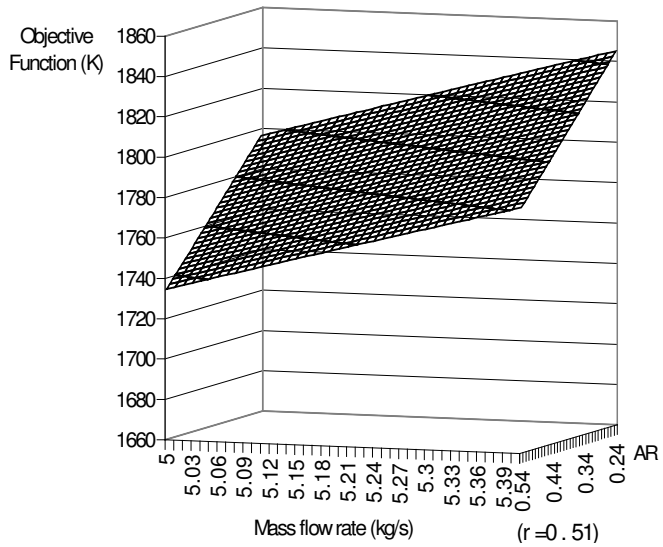

Figure 10 – (b) – Full solutions of the objective function over 1780K (view 1)

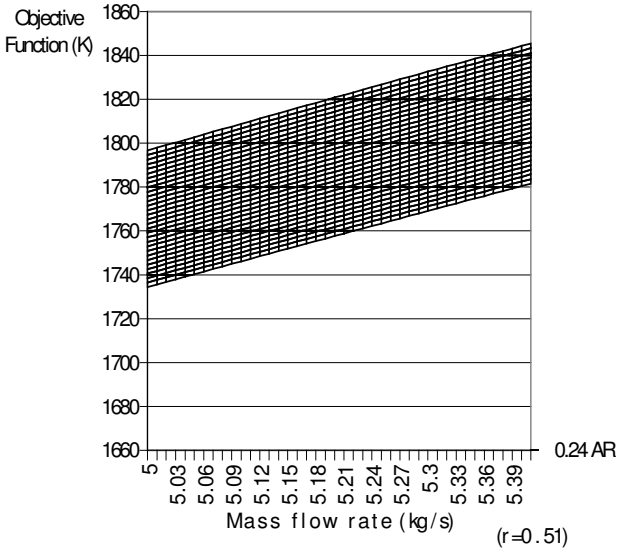

Figure 10 – (c) – Full solutions of the objective function over 1780K (view 2)

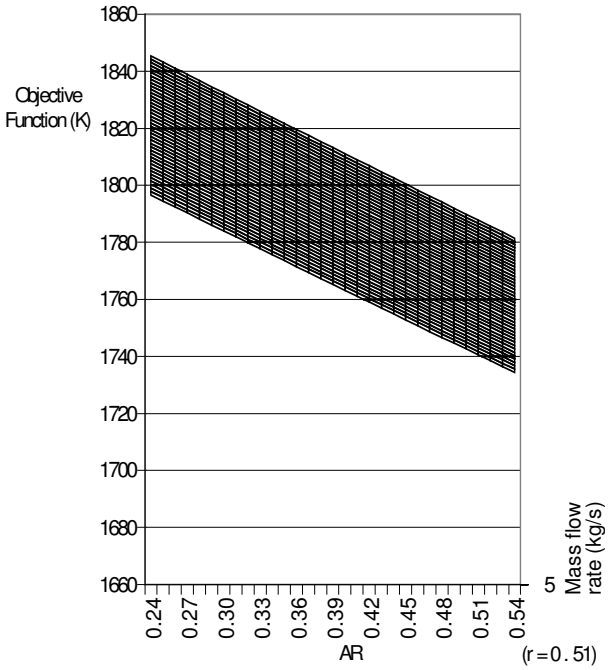

Figure 10 – (d) – Full solutions of the objective function over 1780K (view 3)